ACS APPLIED MATERIALS & INTERFACES

Research Article

www.acsami.org

Tuning the SERS Response with Ag-Au Nanoparticle-Embedded Polymer Thin Film Substrates

V. Kesava Rao and T. P. Radhakrishnan*

School of Chemistry, University of Hyderabad, Hyderabad 500 046, India

Supporting Information

ABSTRACT: Development of facile routes to the fabrication of thin film substrates with tunable surface enhanced Raman scattering (SERS) efficiency and identification of the optimal conditions for maximizing the enhancement factor (EF) are significant in terms of both fundamental and application aspects of SERS. In the present work, polymer thin films with embedded bimetallic nanoparticles of Ag-Au are fabricated by a simple two-stage protocol. Ag nanoparticles are formed in the first stage, by the *in situ* reduction of silver nitrate by the poly(vinyl alcohol) (PVA) film through mild thermal annealing, without any additional reducing agent. In the second stage, aqueous solutions of chloroauric acid spread on the Ag-PVA thin film under ambient conditions, lead to the galvanic displacement of Ag by Au *in situ* inside the film, and the formation of Ag-Au particles. Evolution of the morphology of the bimetallic nanoparticles into hollow cage structures and the distribution of Au on the nanoparticles are revealed through electron microscopy and energy dispersive X-ray spectroscopy. The localized surface plasmon resonance (LSPR) extinction of the nanocomposite thin film evolves with the Ag-Au composition; theoretical simulation of the extinction spectra provides insight into the observed trends. The Ag-Au-PVA thin films are found to be efficient substrates for SERS. The EF follows the variation of the LSPR extinction vis-à-vis the excitation laser wavelength, but with an offset, and the maximum SERS effect is obtained at very low Au content; experiments with Rhodamine 6G showed EFs on the order of 10^8 and a limit of detection of 0.6 pmol. The present study describes a facile and simple fabrication of a nanocomposite thin film that can be conveniently deployed in SERS investigations, and the utility of the bimetallic system to tune and maximize the EF.

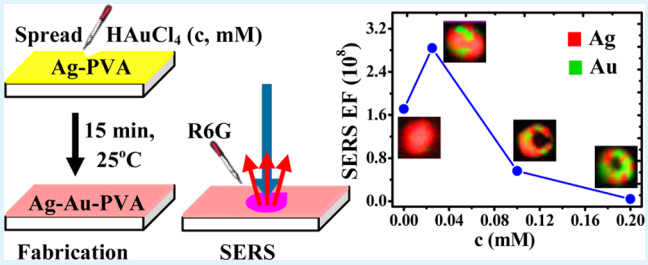

KEYWORDS: *polymer−metal nanocomposite, thin film, silver−gold nanoparticle, in situ fabrication, SERS*

INTRODUCTION

Surface enhanced Raman scattering (SERS) is a phenomenon of great interest and impact from both fundamental science and analytical application perspectives. The inherently weak Raman signal resulting from the two-photon process is enhanced significantly through the influence of the strong local field offered by the substrate surface.[1−5] The SERS effect has been explained in terms of the general mechanism of electromagnetic field enhancement[4−6] as well as the role of chemical enhancement effects[4,5,7,8] in specific cases. While the latter addresses the impact of the substrate surface on the analyte molecule through chemical interactions such as charge transfer, the former is a consequence of the strong local field provided by the surface. Metal nanoparticles, especially those of silver, gold, and copper, with their strong localized surface plasmon resonance (LSPR) fields which can be excited by visible radiation, have been the popular choices for realizing high SERS effects.

The SERS response is critically dependent on the impact of the local electric field on the exciting (frequency = ν_I) and scattered (frequency = ν_R) photons in the Raman process [$\Delta\nu_{Stokes/Anti\text{-}Stokes} = \pm(\nu_I - \nu_R)$]. Therefore, the SERS enhancement factor (EF) due to a metal nanoparticle based substrate is likely to be influenced by the correlation between the LSPR energy and the exciting laser energy. Wavelength-scan studies with different substrates have shown that maximum enhancement occurs when the LSPR peak is approximately midway between the ν_I and ν_R; for Stokes lines in the Raman spectrum, maximum EF is obtained when the LSPR peak is slightly red-shifted with respect to the exciting laser wavelength.[9,10] However, several studies show that the correlation between the LSPR extinction and the SERS EF is not so straightforward. The link between the LSPR extinction and the SERS can be quite indirect, and the spatial distribution of resonance plays a significant role, with the bulk-like character of the collective resonance at a specific wavelength contributing to the extinction and the surface-like character to the SERS.[11] The inherent competition between extinction and enhancement can lead to maximum signals off-resonance, at optimal concentrations in colloidal media, and in particular when the LSPR is blue-shifted with respect to ν_I.[12,13] Another factor of fundamental relevance in this context is that the extinction is

Received: February 23, 2015
Accepted: May 22, 2015
Published: June 2, 2015

DOI: 10.1021/acsami.5b04180
ACS Appl. Mater. Interfaces 2015, 7, 12767−12773

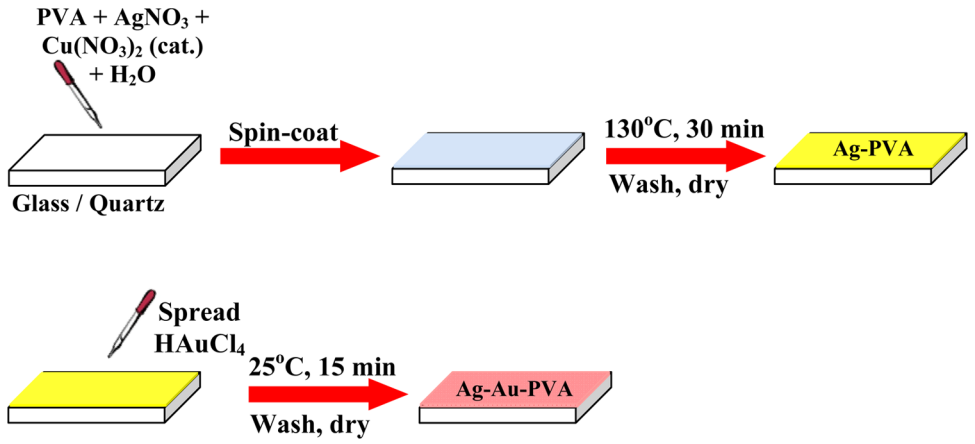

Figure 1. Schematic diagram showing the *in situ* synthesis of Ag-PVA followed by Ag-Au-PVA thin film.

controlled by the far-field behavior of the plasmonic substrate while the SERS response is determined by the near-field effects which once again makes the correlation between the two responses complex.[14] A major focus in the development of SERS substrates has been the generation of large local fields through the formation of features such as "hot spots".[15,16] The impact of cluster size and interparticle separation in nanoparticle aggregates on the near-field enhancement and the design of ultrasensitive plasmonic nanostructures for SERS have been investigated in detail.[17,18] From an alternate perspective, the facility with which the LSPR of metal nanoparticles can be systematically tailored through various methods allows fundamental studies of SERS EF tuning and optimization of the substrate to realize maximum enhancement. LSPR of metal nanoparticles such as gold and silver have been tuned by varying their size and shape, and different aspects of their assembly.[19−23]

Formation of bimetallic nanoparticle offers a facile route to optimize the properties of nanometals. This has been extensively explored in the prototypical system of silver−gold.[24−26] The following aspects require careful consideration from the point of view of SERS. A silver nanoparticle with significantly higher LSPR extinction coefficient than that of gold is often the preferred choice; however, the relatively higher chemical reactivity of silver is an aspect of concern for practical applications, and alloying with gold is generally desirable on this count. Variation of the composition of the bimetallic system can be exploited to tune the LSPR response and hence the SERS effect; it would be greatly advantageous if incorporation of small amounts of gold in the silver nanoparticles increases the EF for commonly used Raman excitation laser wavelengths. As an analytical tool, it is practically very useful to deploy solid SERS substrates, preferably based on polymer thin films fabricated through simple solution routes.

Most of the fundamental and application requirements highlighted above, for realizing an efficient SERS response, can be met using *in situ* fabricated polymer−metal nanocomposite thin films.[27,28] The simple method developed in our laboratory allows the generation of a homogeneous distribution of nanoparticles of noble metals such as silver,[29] gold,[30] and palladium,[31] and also uncommon and unique materials like nanodrops of mercury,[32] within a thin polymer film, through the *in situ* reduction of the metal ions by the polymer itself. The method uses aqueous media and mild processing conditions, and avoids external reducing agents as well as exposure of the generated nanoparticles. Recently the protocol has been extended to generate bimetallic nanoparticles of Ag−Pd through an ambient temperature, template-mediated galvanic displacement procedure.[33]

Following the method we had developed for Ag−Pd nanoparticles, a protocol is now optimized for the fabrication of Ag-Au nanoparticles with systematically varied composition, generated *in situ* inside poly(vinyl alcohol) (PVA) thin film. Ag-PVA thin film containing a uniform distribution of Ag nanoparticles is fabricated in the first stage by the reduction of $AgNO_3$ inside solid PVA film catalyzed by a small amount of $Cu(NO_3)_2$. Spreading the required amount of $HAuCl_4$ solution on the Ag-PVA film under ambient conditions followed by simple washing led to the formation of Ag-Au-PVA thin film. The LSPR peak could be tuned from ∼430 to ∼760 nm by increasing the concentration of the $HAuCl_4$ solution up to ∼0.15 mM. Evolution of the composition and morphology of the alloy nanoparticles is explored using ICP analysis, TEM, FE-SEM, and EDX spectroscopy and mapping. SERS experiments are conducted using Rhodamine 6G (R6G) as the probe molecule on the substrates having varying Ag-Au composition and exhibiting smoothly evolving LSPR peak. With 488 nm excitation laser, the EF is found to increase briefly with increasing Au content but then fall off at higher values. The relation with the LSPR peaks of the substrates is discussed.

RESULTS AND DISCUSSION

The two-step fabrication methodology (see Experimental Section for details) is shown schematically in Figure 1. The first stage is the *in situ* formation of Ag nanoparticles inside the PVA matrix; the fabrication involves aqueous solutions and simple spin-coating followed by thermal annealing under mild conditions. As shown in our earlier study,[33] introduction of a catalytic amount of Cu^{2+} ion enabled the formation of relatively large (30−40 nm) Ag nanoparticles within the PVA thin film matrix. In the second stage, the galvanic displacement of Ag by Au atoms occurs, once again as an *in situ* process, under ambient conditions. Treatment with $HAuCl_4$ solutions of different concentrations (c = 0.005 to 0.2 mM) led to the formation of Ag-Au nanoparticles. The final thin films are typically about 200 nm thick. The Ag-Au composition was analyzed using ICP-OES; films prepared with increasing concentrations of $HAuCl_4$ showed increasing content of Au,

DOI: 10.1021/acsami.5b04180
ACS Appl. Mater. Interfaces 2015, 7, 12767−12773

with a maximum of ~5.4 atom % in the film fabricated with c = 0.2 mM.[34]

Systematic evolution of the LSPR extinction of the polymer−metal nanocomposite thin films as the nanoparticles change from pure Ag to Ag-Au with increasing Au content is shown in Figure 2. The peak at 434 nm observed with the original Ag-PVA shifts gradually up to 761 nm in the case of Ag-Au-PVA prepared using a 0.15 mM solution of $HAuCl_4$ (Table 1). There

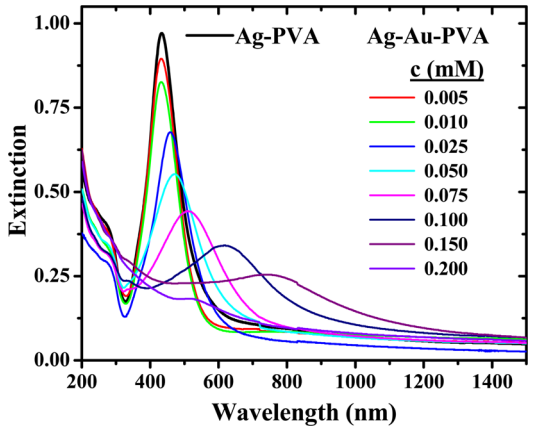

Figure 2. Optical extinction spectra of Ag-PVA and Ag-Au-PVA thin films formed by treating Ag-PVA with different concentrations (c, mM) of $HAuCl_4$ solution.

Table 1. LSPR Peak Wavelength (λ_{max}), Magnitude of the Frequency Difference between the Exciting Laser and the LSPR Peak ($|\Delta\nu|$), and SERS EF for R6G Samples Spread on Ag-PVA and Ag-Au-PVA Prepared Using Different Concentrations (c, mM) of $HAuCl_4$ Solution

c (mM)	λ_{max} (nm)	$\lvert\Delta\nu\rvert$ (cm^{-1})	SERS EF (10^8)
0.000	434	2549. 7	1.71
0.005	434	2549. 7	1.86
0.010	434	2549. 7	2.15
0.025	459	1294.7	2.84
0.050	473	649.9	2.27
0.075	517	1149.4	1.39
0.100	628	4568.2	0.56
0.150	761	7351.2	0.02
0.200	522	1334.7	0.04

is a concomitant and steady decrease in the intensity of the extinction peak; this is mainly a consequence of the relatively lower extinction coefficient of Au compared to Ag. In order to gain insight into the evolution of the spectral profiles and peak shifts, we have carried out computational simulation of the LSPR extinction spectra[34] using the DDSCAT software that employs the discrete dipole approximation.[35,36] Formation of hollow structures with decreasing shell thickness causes significant red shift and broadening of the LSPR peak. The red shift observed in the films with relatively low fractions of Au (fabricated with $c \leq 0.05$ mM) is in good agreement with the computed values; however, at larger fractions of Au, the computed values are significantly lower than those observed experimentally.[34] Computations on hollow Au spheres suggest that the latter discrepancy may be due to the formation of thin Au shells through partial separation of Au. On further increase of Au (c = 0.20 mM), the LSPR peak blue shifts to ~522 nm, indicative of extinction due to solid Au nanostructures with no noticeable intensity due to Au−Ag; this could be due to the formation of Au patches over the Ag-Au nanoparticle. It is pertinent to note that several earlier studies have reported similar observations of blue shift in the LSPR peak of Ag-Au nanoparticles upon enhancing the Au content significantly, and attributed it to the fragmentation of the nanostructures.[37−40] Tuning of the LSPR peak forms the basis for the SERS studies discussed later.

Evolution of the morphology of the nanoparticles with increasing Au content is revealed by the TEM images in Figure 3; selected area electron diffraction shows that these particles

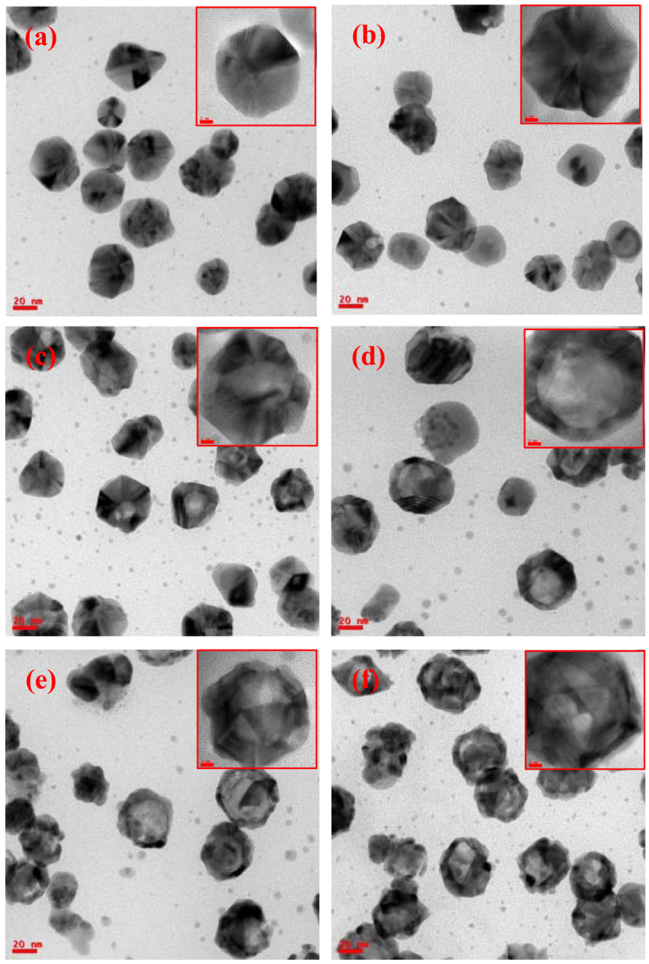

Figure 3. TEM images of (a) Ag-PVA and Ag-Au-PVA thin films formed by treating Ag-PVA with different concentrations (c, mM) of $HAuCl_4$ solution: (b) 0.025, (c) 0.05, (d) 0.10, (e) 0.15, and (f) 0.20. Scale bar = 20 nm; more magnified images (scale bar = 5 nm) of single particle are shown in the inset.

are crystalline.[34] Formation of the hollow cage structures at higher Au content is seen in the more magnified images. The hollow structures appear to result from the Kirkendall effect[41] arising due to the different rates of diffusion of the two kinds of atoms/ions involved; similar observations have been made earlier with Ag−Pd[33] as well as Ag-Au[37] nanoparticles. The increasing surface roughness could support applications such as catalysis or SERS. The FE-SEM images of the Ag-Au nanoparticles embedded in the PVA thin film (Figure 4) reveal morphological changes similar to that observed in the TEM images. The EDX line profile is consistent with the hollow

DOI: 10.1021/acsami.5b04180
ACS Appl. Mater. Interfaces 2015, 7, 12767−12773

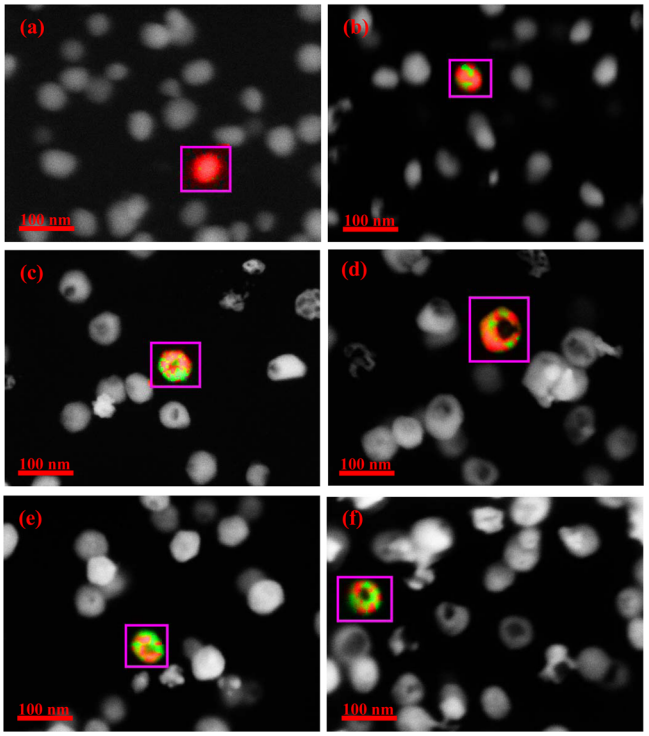

Figure 4. FE-SEM images combined with EDX area mapping of (a) Ag-PVA and Ag-Au-PVA thin films formed by treating Ag-PVA with different concentrations (c, mM) of $HAuCl_4$ solution: (b) 0.025, (c) 0.05, (d) 0.10, (e) 0.15, and (f) 0.20; scale bar = 100 nm. The EDX mapping shows Ag (red) and Au (green) regions in a selected particle.

structure of the particles and provides insight into the elemental distribution.[34] The area mapping of single particles shows graphically the increasing Au content and the distribution of Au on the Ag nanoparticles (Figure 4). Quantitative estimates of the Au content across the series follow the same trend as observed from the ICP analysis, but show relatively higher values;[34] such differences are well-known[42] and attributable to the fact that the EDX probes primarily the surface composition whereas the ICP analyzes the total content.

R6G was used as the analyte molecule in the SERS studies on the Ag-Au-PVA thin film substrates (coated on Si wafer). A sample of microcrystalline R6G served as the reference for estimating the SERS EF. The Raman spectra of R6G reference sample and solutions adsorbed on the Ag-PVA and Ag-Au-PVA films were recorded in a confocal microscope. The protocol that we have optimized for the preparation of samples on the SERS substrate is particularly convenient as the analyte solution is simply spread on the nanocomposite thin film and allowed to adsorb; this may be contrasted with methods such as incubation required in some of the earlier studies.[9,10] The spectra of R6G recorded using the Ag-Au-PVA thin films with low Au content were found to increase slightly in intensity with time and reach steady values after ~24 h; the relative SERS intensities across the substrates with different compositions remain the same, however. As the LSPR spectra of these Ag-Au-PVA films are reproducible over several days, we believe that the spectral changes occur due to the progress of the analyte adsorption on the nanoparticles reaching an equilibrium over several hours. The Raman spectra of R6G recorded on different substrates after 24 h are displayed in Figure 5. Peaks in the spectrum of the reference R6G sample spectrum are hardly visible, but can

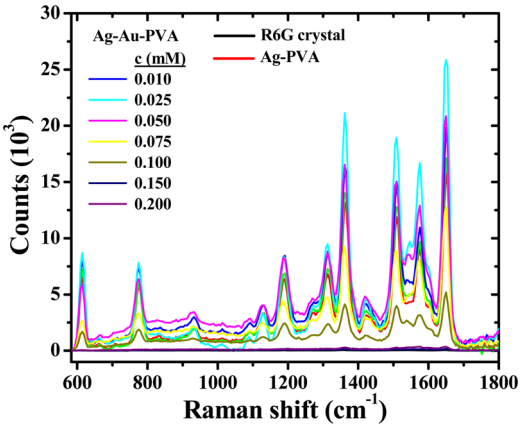

Figure 5. Raman spectra of R6G microcrystals and solution adsorbed on Ag-PVA thin film and Ag-Au-PVA thin films formed by treating Ag-PVA with different concentrations (c, mM) of $HAuCl_4$ solution.

be discerned on magnification, allowing the quantitative estimation of the EF. A relatively low spectral profile is obtained with Ag-PVA as the substrate. With increasing Au content, intensities of all the peaks increase, reach a maximum, and thereafter decrease steadily.

The EF values estimated for the different substrates are collected in Table 1; intensity of the 1645−1650 cm^{-1} peak due to the aromatic C−C stretch vibration was used for the estimation (see the Experimental Section for details),[34] and the EF values are typically ~10^8. Figure 6 shows the variation of the

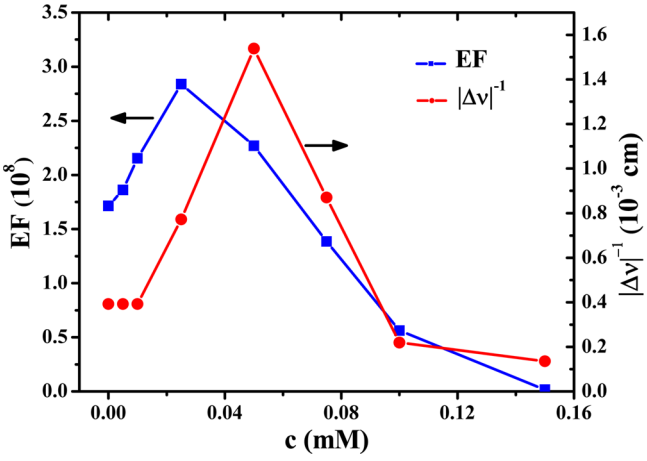

Figure 6. Plot of the SERS EF and $|\Delta\nu|^{-1}$ against the concentration (c, mM) of $HAuCl_4$ used to prepare the Ag-Au-PVA thin film (c = 0 corresponds to the Ag-PVA thin film): $\Delta\nu = \nu_I - \nu_{LSPR}$ where ν_I = frequency of the excitation laser, ν_{LSPR} = frequency of the LSPR peak for the Ag-PVA or Ag-Au-PVA thin film.

EF with the concentration (c, mM) of $HAuCl_4$ used in the fabrication of the substrate. The maximum value of 2.84×10^8 is ~70% higher than that obtained with Ag-PVA as the substrate, and is achieved using the Ag-Au-PVA thin film substrate containing 2.77 atom % of Au (based on EDX (TEM) analysis), corresponding to c = 0.025 mM. Figure 6 shows also the plot of $|\Delta\nu|^{-1}$ against c: $\Delta\nu = \nu_I - \nu_{LSPR}$ where ν_I corresponds to the frequency of the excitation laser (λ = 488 nm) and ν_{LSPR} is the frequency of the LSPR peak for each substrate. The maximum EF is obtained with the substrate having an LSPR peak that is slightly blue-shifted with respect to

DOI: 10.1021/acsami.5b04180
ACS Appl. Mater. Interfaces 2015, 7, 12767−12773

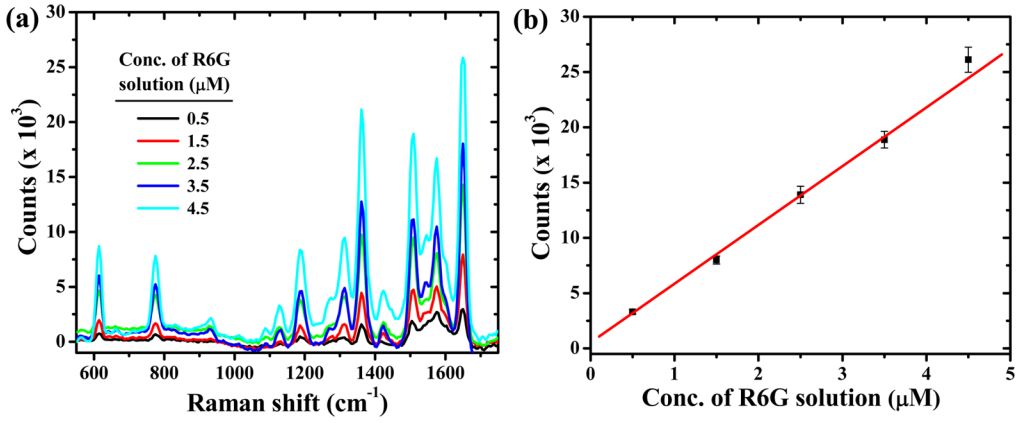

Figure 7. (a) Raman spectra of R6G solutions with different concentrations adsorbed on Ag-Au-PVA thin film (c = 0.025 mM of $HAuCl_4$) and (b) plot of the intensity of the 1650 cm^{-1} peak as a function of the concentration of R6G solution (the least-square fit line is also shown).

the excitation laser, rather than with the substrate that has a nearly resonant LSPR (i.e., with the lowest $\Delta\nu$). This observation is similar to that reported earlier with Au nanosphere[12] and nanostar[13] based colloidal substrates; however, we believe that the maximization of the enhancement off-resonance with respect to the exciting radiation does not arise due to a competition between the extinction and enhancement effects for the following reasons. In the present case, we are working with a planar substrate rather than a colloidal suspension. More importantly, the extinction is found to gradually decrease as the Au content increases (Figure 2) consistent with the simulations based on hollow alloy nanoparticles described above.[34] A subtle trade-off between resonance and extinction appears to lead to the maximization of the SERS EF. Incorporation of small but increasing amounts of Au into Ag moves the LSPR peak closer to the excitation wavelength, but concomitantly decreases the extinction peak intensity; the opposing impacts of the two factors leads to a maximization of the EF at an intermediate Au content. A similar observation in an earlier study,[43] of maximum SERS response with Ag-Au core−shell nanoparticles having intermediate composition, has been attributed to the maximization of pinhole formation. In the present case, as the thickness of the nanocomposite film is ∼200 nm and the Ag-Au nanoparticles are 40−50 nm in diameter (slightly larger than the Ag nanoparticles), the close contact of particles can give rise to regions of high local electric field and contribute to enhanced SERS effects.

SERS experiments on several samples of Ag-Au-PVA substrate and multiple measurements on each sample showed a high level of reproducibility.[34] Experiments were carried out with different concentrations of R6G solutions on the film having the optimal Au concentration (fabricated with c = 0.025 mM); the spectra recorded and the plot of the intensity of the 1650 cm^{-1} peak as a function of the concentration of the R6G solution, including the standard deviation in each case, are shown in Figure 7. The limit of detection (defined as $3\sigma_{blank}/m$ where σ_{blank} is the standard deviation for blank measurements and m is the slope of the intensity−concentration plot)[44,45] was found to be 0.6 pmol.[34] It may be noted that this value is based on the total solution spread on the substrate; the value would be still lower if only those in the focal volume are considered. The fact that the maximum EF is obtained at very low concentrations of Au in the Ag-Au-PVA is of great practical utility in terms of cost-effectiveness of the substrate. The ease of fabrication and utilization of the *in situ* fabricated polymer-bimetal nanocomposite thin films is an added benefit.

CONCLUSIONS

A simple protocol for the *in situ* fabrication of Ag-Au nanoparticles with hollow cage structures and systematically varied composition, embedded within a PVA thin film, is developed. The Ag-Au-PVA thin films exhibit a systematically tuned LSPR peak across a range of ∼330 nm. These nanocomposite thin films are used as substrates for SERS experiments with Rhodamine 6G as the analyte molecule. Enhancement factors of $\sim 10^8$ are obtained. The maximum EF is observed with the substrate having a relatively small Au content. This substrate shows an LSPR extinction peak blue-shifted with respect to the laser excitation wavelength, highlighting the trade-off between the extinction and resonance leading to maximum SERS response. The utility of LSPR tuning in easily fabricated bimetallic nanoparticle-embedded polymer thin films, leading to the fabrication of efficient SERS substrates, is demonstrated.

EXPERIMENTAL SECTION

Fabrication of Ag-PVA Film. A 0.32 g portion of $AgNO_3$ (Aldrich, purity = 99.9999%) dissolved in 2 mL of water was mixed with a solution of 0.25 g of PVA (Aldrich, average molecular weight = 146−186 kDa, % hydrolysis = 99+) in 5 mL of water. A 10.8 mg portion of $Cu(NO_3)_2{\cdot}3H_2O$ was dissolved in this solution; the weight % of copper in terms of the total metal (Ag + Cu) content is ∼1.4. All the solutions were prepared using Millipore Milli-Q water (resistivity = 18.2 MΩ cm). Glass/quartz/Si wafer substrates were cleaned by washing and sonication in isopropyl alcohol, and dried. The solution mixture was spin-coated on the substrate using a Laurell Technologies Corporation Model WS-650HZ-23NPP/LITE photoresist spinner at 500 rpm for 10 s followed by 6000 rpm for 10 s. The film was heated at 130 °C for 30 min and then washed with ∼1 mL of water and dried under ambient atmosphere.

Fabrication of Ag-Au-PVA Film. A ∼0.5 mL portion of aqueous solutions of $HAuCl_4$ with concentrations ranging from 0.005 to 0.200 mM was spread uniformly on the Ag-PVA film and kept for 15 min under ambient temperature (∼25 °C) conditions, inside a closed Petri dish to avoid evaporation. The film was then washed with ∼1 mL of water and dried under vacuum for 1 h. Thickness of the final films was measured using an Ambios Technology XP-1 profilometer.

Characterization of the Polymer−Metal Nanocomposite Thin Films. Chemical composition of the film was analyzed using a Varian Model Liberty Series inductively coupled plasma-optical emission spectrometer (ICP-OES). Sample for the analysis was

DOI: 10.1021/acsami.5b04180
ACS Appl. Mater. Interfaces 2015, 7, 12767−12773

prepared by dissolving the film in 100 mL of 69% nitric acid. Electronic spectra of the nanocomposite thin films were recorded on a Varian Model Cary 100 UV−vis spectrometer or a Shimadzu Model UV-3600 UV−vis−NIR spectrometer. Transmission electron microscopy (TEM) was carried out on a FEI TECNAI G^2 S-Twin TEM at an accelerating voltage of 200 kV. For the preparation of free-standing films for TEM and FE-SEM imaging the substrate was first coated with a few drops of a solution of polystyrene (Aldrich, average molecular weight = 280 kDa) in toluene (1 g in 7 mL) by spinning at 1000 rpm for 10 s and dried in a hot air oven at 90 °C for 15 min. This substrate was used for the fabrication of the Ag-PVA or Ag-Au-PVA film. The multilayer film obtained was peeled off the glass substrate, placed on a 200 mesh copper grid, and then dipped in toluene, whereupon the polystyrene layer dissolves and the nanocomposite Ag-PVA or Ag-Au-PVA film sticks to the grid. Field emission scanning electron microscope (FE-SEM) imaging with energy dispersive X-ray (EDX) spectroscopy was carried out on a Carl Zeiss model Ultra 55 microscope; EDX spectra and maps were recorded using Oxford Instruments X-Max^N SDD (50 mm^2) system and INCA analysis software.

SERS Experiments. Experiments were conducted using Ag-PVA as well as Ag-Au-PVA (with different Au content) coated on silicon wafer, as the SERS substrate. Rhodamine 6G (R6G) was used as the analyte molecule; 20 μL of a 4.5 μM solution of R6G in methanol was spread uniformly on the substrate and dried under ambient atmosphere. A WITec model Alpha 300 R Raman microscope (with AFM) was used for recording the Raman spectra, with 0.5 s integration time and 10 accumulations, through a 20× aperture (NA = 0.4). A 488 nm laser was used as the excitation source. The laser intensity was maintained constant in all measurements; a 100 μm detecting fiber was used to collect the spectra. A Raman spectrum for the bulk material used as the reference was recorded using a small R6G microcrystal placed on the Si wafer. The number of molecules in the reference sample (N_{BULK}) was determined using the focal volume of the laser spot incident on the microcrystal and the density of the material. The number of molecules in the sample (N_{SERS}) was estimated by considering the total number of molecules spread on the substrate, assuming a homogeneous distribution across the thin film and the fraction falling within the laser spot area. Intensity of the aromatic C−C stretch vibration in the reference sample at 1645 cm^{-1} (I_{BULK}) and in the solutions on the Ag-PVA and Ag-Au-PVA substrates at 1650 cm^{-1} (I_{SERS}) was used to estimate the enhancement factor, EF = $(N_{BULK}/N_{SERS}) \times (I_{SERS}/I_{BULK})$.[34] As N_{SERS} includes all the probe molecules in the focal volume and not just a monolayer on the nanoparticles, the EF reported is the lower bound of this value.

■ ASSOCIATED CONTENT

Supporting Information

Details of elemental composition analysis, SAED and EDX line profile images of Ag-Au-PVA films, simulation of the LSPR extinction spectra, calculation of the EF values for Ag-Au-PVA thin films with varying composition, and estimation of the limit of detection. The Supporting Information is available free of charge on the ACS Publications website at DOI: 10.1021/acsami.5b04180.

■ AUTHOR INFORMATION

Corresponding Author

*E-mail: tpr@uohyd.ac.in. Fax: 91-40-2301-2460. Phone: 91-40-2313-4827.

Notes

The authors declare no competing financial interest.

■ ACKNOWLEDGMENTS

Financial support from the Department of Science and Technology and the University Grants Commission, New Delhi, and infrastructure support from the Centre for Nanotechnology and FE-SEM facility (School of Chemistry) at the University of Hyderabad are acknowledged with gratitude. We thank Mr. M. Durga Prasad and Mr. D. Sunil for help with the TEM and FE-SEM imaging, respectively. V.K.R. thanks the UGC, New Delhi, for a senior research fellowship.

■ REFERENCES

(1) Fleischman, M.; Hendra, P. J.; McQuillan, A. J. Raman-Spectra of Pyridine Adsorbed at a Silver Electrode. *Chem. Phys. Lett.* **1974**, *26*, 163−166.

(2) Jeanmaire, D. L.; Van Duyne, R. P. Surface Raman Spectroelectrochemistry. 1. Heterocyclic, Aromatic, and Aliphatic-Amines Adsorbed on Anodized Silver Electrode. *J. Electroanal. Chem.* **1977**, *84*, 1−20.

(3) Albrecht, M. G.; Creighton, J. A. Anomalously Intense Raman Spectra of Pyridine at a Silver Electrode. *J. Am. Chem. Soc.* **1977**, *99*, 5215−5217.

(4) Campion, A.; Kambhampati, P. Surface-Enhanced Raman Scattering. *Chem. Soc. Rev.* **1998**, *27*, 241−250.

(5) Kneipp, K.; Kneipp, H.; Kneipp, J. Surface-Enhanced Raman Scattering in Local Optical Fields of Silver and Gold Nanoaggregatess from Single-Molecule Raman Spectroscopy to Ultrasensitive Probing in Live Cells. *Acc. Chem. Res.* **2006**, *39*, 443−450.

(6) Wang, W.; Li, Z.; Gu, B.; Zhang, Z.; Xu, H. Ag@SiO2 Core-Shell Nanoparticles for Probing Spatial Distribution of Electromagnetic Field Enhancement via Surface-Enhanced Raman Scattering. *ACS Nano* **2009**, *3*, 3493−3496.

(7) Campion, A.; Ivanecky, J. E.; Child, C. M.; Foster, M. On the Mechanism of Chemical Enhancement in Surface-Enhanced Raman Scattering. *J. Am. Chem. Soc.* **1995**, *117*, 11807−11808.

(8) Uetsuki, K.; Verma, P.; Yano, T.; Saito, Y.; Ichimura, T.; Kawata, S. Experimental Identification of Chemical Effects in Surface Enhanced Raman Scattering of 4-Aminothiophenol. *J. Phys. Chem. C* **2010**, *114*, 7515−7520.

(9) McFarland, A. D.; Young, M. A.; Dieringer, J. A.; Van Duyne, R. P. Wavelength-Scanned Surface-Enhanced Raman Excitation Spectroscopy. *J. Phys. Chem. B* **2005**, *109*, 11279−11285.

(10) Zhao, J.; Dieringer, J. A.; Zhang, X.; Schatz, G. C.; Van Duyne, R. P. Wavelength-Scanned Surface-Enhanced Resonance Raman Excitation Spectroscopy. *J. Phys. Chem. C* **2008**, *112*, 19302−19310.

(11) Le Ru, E. C.; Galloway, C.; Etchegoin, P. G. On the Connection between Optical Absorption/Extinction and SERS Enhancements. *Phys. Chem. Chem. Phys.* **2006**, *8*, 3083−3087.

(12) van Dijk, T.; Sivapalan, S. T.; DeVetter, B. M.; Yang, T. K.; Schulmerich, M. V.; Murphy, C. J.; Bhargava, R.; Carney, P. S. Competition between Extinction and Enhancement in Surface-Enhanced Raman Spectroscopy. *J. Phys. Chem. Lett.* **2013**, *4*, 1193−1196.

(13) Li, M.; Kang, J. W.; Dasari, R. R.; Barman, I. Shedding Light on the Extinction-Enhancement Duality in Gold Nanostar-Enhanced Raman Spectroscopy. *Angew. Chem., Int. Ed.* **2014**, *53*, 14115−14119.

(14) Doherty, M. D.; Murphy, A.; Pollard, R. J.; Dawson, P. Surface-Enhanced Raman Scattering from Metallic Nanostructures: Bridging the Gap between the Near-Field and Far-Field Responses. *Phys. Rev. X* **2013**, *3*, 011001.

(15) Lee, S. J.; Morrill, A. R.; Moskovits, M. Hot Spots in Silver Nanowire Bundles for Surface-Enhanced Raman Spectroscopy. *J. Am. Chem. Soc.* **2006**, *128*, 2200−2201.

(16) Wang, H.; Levin, C. S.; Halas, N. J. Nanosphere Arrays with Controlled Sub-10-nm Gaps as Surface-Enhanced Raman Spectroscopy Substrates. *J. Am. Chem. Soc.* **2005**, *127*, 14992−14993.

(17) Fraire, J. C.; Pérez, L. A.; Coronado, E. A. Cluster Size Effects in the Surface-Enhanced Raman Scattering Response of Ag and Au Nanoparticle Aggregates: Experimental and Theoretical Insight. *J. Phys. Chem. C* **2013**, *117*, 23090−23107.

DOI: 10.1021/acsami.5b04180
ACS Appl. Mater. Interfaces 2015, 7, 12767−12773

(18) Fraire, J. C.; Pérez, L. A.; Coronado, E. A. Rational Design of Plasmonic Nanostructures for Biomolecular Detection: Interplay Between Theory and Experiments. *ACS Nano* **2012**, *6*, 3441−3452.
(19) Angelome, P. C.; Mezerji, H. H.; Goris, B.; Pastoriza-Santos, I.; Pérez-Juste, J.; Bals, S.; Liz-Marzán, L. M. Seedless Synthesis of Single Crystalline Au Nanoparticles with Unusual Shapes and Tunable LSPR in the Near-IR. *Chem. Mater.* **2012**, *24*, 1393−1399.
(20) Jensen, T. R.; Malinsky, M. D.; Haynes, C. L.; Van Duyne, R. P. Nanosphere Lithography: Tunable Localized Surface Plasmon Resonance Spectra of Silver Nanoparticles. *J. Phys. Chem. B* **2000**, *104*, 10549−10556.
(21) Kelly, K. L.; Coronado, E.; Zhao, L. L.; Schatz, G. C. The Optical Properties of Metal Nanoparticles: The Influence of Size, Shape, and Dielectric Environment. *J. Phys. Chem. B* **2003**, *107*, 668−677.
(22) Zhang, X.; Hicks, E. M.; Zhao, J.; Schatz, G. C.; Van Duyne, R. P. Electrochemical Tuning of Silver Nanoparticles Fabricated by Nanosphere Lithography. *Nano Lett.* **2005**, *5*, 1503−1507.
(23) Wiley, B. J.; Im, S. H.; Li, Z. Y.; McLellan, J.; Siekkinen, A.; Xia, Y. Maneuvering the Surface Plasmon Resonance of Silver Nanostructures through Shape-Controlled Synthesis. *J. Phys. Chem. B* **2006**, *110*, 15666−15675.
(24) Rycenga, M.; Hou, K. K.; Cobley, C. M.; Schwartz, A. G.; Camargo, P. H. C.; Xia, Y. Probing the Surface-Enhanced Raman Scattering Properties of Au-Ag Nanocages at Two Different Excitation Wavelengths. *Phys. Chem. Chem. Phys.* **2009**, *11*, 5903−5908.
(25) Petri, M. V.; Ando, R. A.; Camargo, P. H.C. Tailoring the Structure, Composition, Optical Properties and Catalytic Activity of Ag-Au Nanoparticles by the Galvanic Replacement Reaction. *Chem. Phys. Lett.* **2012**, *531*, 188−192.
(26) Bu, Y.; Lee, S. Influence of Dopamine Concentration and Surface Coverage of Au Shell on the Optical Properties of Au, Ag, and $Ag_{core}Au_{shell}$ Nanoparticles. *ACS Appl. Mater. Interfaces* **2012**, *4*, 3923−3931.
(27) Ramesh, G. V.; Porel, S.; Radhakrishnan, T. P. Polymer Thin Films Embedded with in Situ Grown Metal Nanoparticles. *Chem. Soc. Rev.* **2009**, *38*, 2646−2656.
(28) Hariprasad, E.; Radhakrishnan, T. P. *In Situ* Fabricated Polymer−Silver Nanocomposite Thin Film as an Inexpensive and Efficient Substrate for Surface-Enhanced Raman Scattering. *Langmuir* **2013**, *29*, 13050−13057.
(29) Porel, S.; Singh, S.; Harsha, S. S.; Rao, D. N.; Radhakrishnan, T. P. Nanoparticle-Embedded Polymer: In Situ Synthesis, Free-standing Films with Highly Monodisperse Silver Nanoparticles and Optical Limiting. *Chem. Mater.* **2005**, *17*, 9−12.
(30) Porel, S.; Singh, S.; Radhakrishnan, T. P. Polygonal Gold Nanoplates in a Polymer Matrix. *Chem. Commun.* **2005**, 2387−2389.
(31) Hariprasad, E.; Radhakrishnan, T. P. Palladium Nanoparticle-Embedded Polymer Thin Film "Dip Catalyst" for Suzuki−Miyaura Reaction. *ACS Catal.* **2012**, *2*, 1179−1186.
(32) Ramesh, G. V.; Prasad, M. D.; Radhakrishnan, T. P. Mercury Nanodrops and Nanocrystals. *Chem. Mater.* **2011**, *23*, 5231−5236.
(33) Rao, V. K.; Radhakrishnan, T. P. Hollow Bimetallic Nanoparticles Generated in situ Inside a Polymer Thin Film: Fabrication and Catalytic Application of Silver−Palladium−Poly(vinyl alcohol). *J. Mater. Chem. A* **2013**, *1*, 13612−13618.
(34) See Supporting Information.
(35) Draine, B. T.; Flatau, P. J. Discrete-Dipole Approximation for Scattering Calculations. *J. Opt. Soc. Am. A* **1994**, *11*, 1491−1499.
(36) *DDSCAT (Version 7.3)* available from http://code.google.com/p/ddscat/.
(37) Sun, Y.; Xia, Y. Mechanistic Study on the Replacement Reaction between Silver Nanostructures and Chloroauric Acid in Aqueous Medium. *J. Am. Chem. Soc.* **2004**, *126*, 3892−3901.
(38) Yang, J.; Lee, J. Y.; Too, H. Core-Shell Ag-Au Nanoparticles from Replacement Reaction in Organic Medium. *J. Phys. Chem. B* **2005**, *109*, 19208−19212.
(39) Zhang, X.; Zhang, G.; Zhang, B.; Su, Z. Synthesis of Hollow Ag-Au Bimetallic Nanoparticles in Polyelectrolyte Multilayers. *Langmuir* **2013**, *29*, 6722−6727.
(40) Polavarapu, L.; Liz-Marzán, L. M. Growth and Galvanic Replacement of Silver Nanocubes in Organic Media. *Nanoscale* **2013**, *5*, 4355−4361.
(41) Gonzalez, E.; Arbiol, J.; Puntes, V. F. Carving at the Nanoscale: Sequential Galvanic Exchange and Kirkendall Growth at Room Temperature. *Science* **2011**, *334*, 1377−1380.
(42) Michalak, I.; Chojnacka, K.; Marycz, K. Using ICP-OES and SEM-EDX in Biosorption Studies. *Michrochim. Acta* **2011**, *173*, 65−74.
(43) Cui, Y.; Ren, B.; Yao, J. L.; Gu, R. A.; Tian, Z. Q. Synthesis of $Ag_{core}Au_{shell}$ Bimetallic Nanoparticles for Immunoassay Based on Surface-Enhanced Raman Spectroscopy. *J. Phys. Chem. B* **2006**, *110*, 4002−4006.
(44) El-Safty, S. A.; Ismail, A. A.; Matsunaga, H.; Nanjo, H.; Mizukami, F. Uniformly Mesocaged Cubic *Fd*3*m* Monoliths as Model Carriers for Optical Chemosensors. *J. Phys. Chem. C* **2008**, *112*, 4825−4835.
(45) Christian, G. D. *Analytical Chemistry*, 6th ed.; John Wiley & Sons Inc.: New York, 2003.

DOI: 10.1021/acsami.5b04180
ACS Appl. Mater. Interfaces 2015, 7, 12767−12773